Accurate Detection of Weld Seams for Laser Welding in Real-World Manufacturing

Rabia Ali[*2], **Muhammad Sarmad** [*1], **Jawad Tayyub** [*2], **Alexander Vogel** [2]

[1] Norwegian University Of Science and Technology, Trondheim, Norway
[2] Endress + Hauser, Germany
rabiaali95.ra@gmail.com, muhammad.sarmad@ntnu.no,
{jawad.tayyub, alexander.vogel}@endress.com

Abstract

Welding is a fabrication process used to join or fuse two mechanical parts. Modern welding machines have automated lasers that follow a pre-defined weld seam path between the two parts to create a bond. Previous efforts have used simple computer vision edge detectors to automatically detect the weld seam edge on an image at the junction of two metals to be welded. However, these systems lack reliability and accuracy resulting in manual human verification of the detected edges. This paper presents a neural network architecture that automatically detects the weld seam edge between two metals with high accuracy. We augment this system with a pre-classifier that filters out anomalous workpieces (e.g., incorrect placement). Finally, we justify our design choices by evaluating against several existing deep network pipelines as well as proof through real-world use. We also describe in detail the process of deploying this system in a real-world shop floor including evaluation and monitoring. We make public a large, well-labeled laser seam dataset to perform deep learning-based edge detection in industrial settings.

Introduction

Welding is an essential process in the manufacturing industry. Commonly, welding is used for fusing two metals or repairing damaged metals. Laser welding is preferred over traditional methods, e.g., tungsten inert gas welding, metal inert gas welding, spot welding, etc., due to its many advantages. These are high precision, low heat-affected zones, high energy density, high welding speed, and low shape distortion. Furthermore, traditional welding methods fail when dealing with very narrow or small weld seams. Laser welding performs better in these cases given its non-contact nature. Thus, laser welding is a robust method widely used in automotive, shipping, aircraft and many other industries.

The accuracy of laser welding is highly dependent on the precise detection of the *welding seam* position between the two parts to be welded. With the widespread use of laser welding, harsh precision requirements with strict weld torch control led to a demand for high-precision weld seam detection technology.

Currently, classic vision algorithms, such as Hough edge detector (Wu et al. 2015), Canny edge detector (Lu, Pan, and Xia 2013), etc., are used to perform weld seam detection on images of the welding pieces. However, these lack the stringent tolerance required for industrial use (see Fig. 1). This leads to constant human intervention to verify and correct every detected edge. This process is both time and labor intensive as well as being detrimental to full automation. Furthermore, following long working hours performing this redundant task leads to deteriorated human judgment and thus low-quality edge detection. Also, different human workers offer different input leading to variation across different weld seams. To fully automate the welding process, an ML-based system is proposed to detect the weld seam to a high accuracy (in our case ± 3 pixels or 0.069 mm) without the need for human verification or correction.

In this paper, we present a weld seam detection method using convolution neural networks (CNNs). The overall method comprises of two modules; edge classification and edge detection. Edge classification classifies a weld seam image as normal or abnormal based on the visual clarity of the edge. This module ensures that spurious images caused by misplacement of parts, blurring, machine errors, etc., are filtered out. The edge detection module utilises a modified U-Net (Ronneberger, Fischer, and Brox 2015) architecture that predicts a weld seam location based on a 1D edge mask. Our architecture is robust and achieves pixel-level precision without human intervention. Remarkably, we achieve a 91 % accuracy on predicting weld seams within a ± 1 pixel (0.023 mm) tolerance. Fig. 1 illustrates the importance of such fine-grained precision for the correct placement of welding material. Our model can be deployed in the laser welding machines used in the industry.

We manually label thousands of weld seam images to create a challenging real-world dataset that directly encapsulates an industrial computer vision problem. All data and code will be made publicly available.

Related Work

In early works, (Bastos et al. 1994) used ultrasonic sensors for detecting weld seams on metal parts. However, operating such sensors in an industrial environment is difficult as they require a stable non-interference state. Arc sensors detect weld seams well (Pan 2001), however narrow weld-

[*]These authors contributed equally.

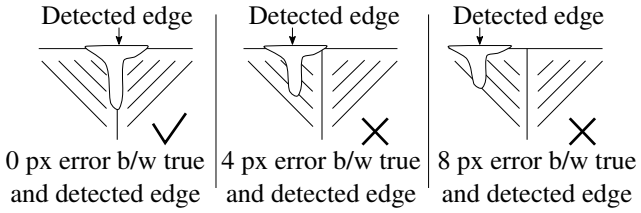

Figure 1: Pixel-level precision is required for seam detection. An error of no more than ± 3 pixels (0.0069mm) is acceptable.

seams pose a problem.

For automatic seam detection, structured light methods based on optical triangulation are commonly used to detect the 3D position of joints with large grooves. Zou et al. (Zou and Chen 2018) projected a structured laser on the workpiece surface and extracted laser stripes from images (strongly disturbed by an arc) to calculate the 3D position of the seam. This was then used to control the motion of the welding torch in real-time. Li et al. (Li et al. 2017) proposed a robust automatic welding seam identification and tracking method by utilizing structured light vision, which can identify deformed laser stripes in a complex welding environment. The position of the welding seam is then found. Some companies have released commercial seam detection sensors based on such structured light methods (Zou and Chen 2018). Industrial products from companies such as Scansonic, Yaskawa, and SERVO-ROBOT are available for implementing structured light vision (Rout, Deepak, and Biswal 2019). For example, the i-CUBE from SERVO-ROBOT is an integrated sensor with a camera and laser projector. It is used to detect the weld seam and implement real-time welding control. The TH6D optical sensor from Scansonic uses multiple light beams to track the hem, and both seam position and gap dimensions are obtained after processing.

However, for narrow seams, the deformation of structured light stripes almost disappears, resulting in a weak detection system (Zeng et al. 2016). Researchers have proposed various methods to solve this problem. In (Xiong et al. 2009), an autonomous welding seam recognition algorithm finds a pair of parallel welding seams in a local area. Then, the remnant edge is sought using iterative edge detection and linking through a shift window constructed from the two endpoints of each edge. In (Micallef, Fang, and Dinham 2011; Pachidis and Lygouras 2007), median filters and smoothing techniques were proposed along with a binary conversion threshold to segment the image leaving only the weld seam visible. However, the weld seam in their experiments and the background are highly contrasting making the seam detection trivial.

Some seam detection algorithms use predefined regions of interest (ROI) (Zou and Zhou 2019). These are introduced to help focus on the weld seam. In (Dinham, Fang, and Zou 2011) a predefined ROI is located in the center of the image. Pixel intensities in a local window are then used to define a threshold for segmenting the weld seam from the background. Similarly, in (Ryberg et al. 2010) an ROI is centered in the image to ignore background artifacts. Although these methods require fewer resources and provide fast seam detection, they do not guarantee pixel-level accuracy.

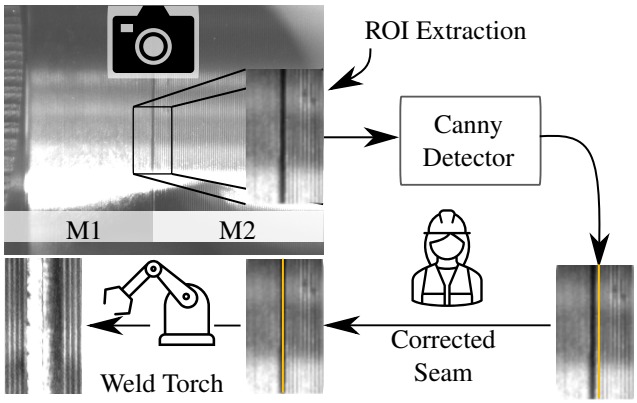

Figure 2: Conventional Method: A Camera takes the image of the two work-pieces M1 and M2, to be welded together. Region of Interest (ROI) is extracted using fixed crops from the center of the picture. The same is fed to the edge detection pipeline. The operator corrects the automatic edge detection by manual adjustment. Finally, the seam is welded by a robotic weld torch.

Methodology

Our pipeline is developed for the automatic weld seam detection of a Trumpf TruLeserCell 3000/5000 laser welding machines[1]. Two parts to be welded are placed in the machine in customized brackets. A camera unit with a light source then takes a full-size picture of these parts, see Fig. 2. This image encapsulates the weld seam visibly. A fixed region of interest (ROI) is then extracted from the image isolating the weld seam area by cropping out background containing shadows, glare, etc. The current method requires correction by a human in the loop for a successful welding process.

Instead, we process the ROI through our edge processing architecture which consists of two modules: an edge classification module $\mathcal{C}$ and an edge detection module $\mathcal{D}$ as shown in Fig. 3. Each module is a deep neural network that is trained separately. In the following subsections, we explain each of these in further detail.

Edge Classification $\mathcal{C}$

The edge classification module is a simple binary classifier that classifies an edge as normal or abnormal, see Fig. 3 part (a). Input to this module is an $H \times W$ ROI image, and output is a label specifying either a 1 (normal) or 0 (abnormal) image. An edge is abnormal if the image lacks clarity or a

[1]https://www.trumpf.com/en_GB/products/machines-systems/laser-welding-systems-and-the-arc-welding-cell/trulaser-cell-3000/

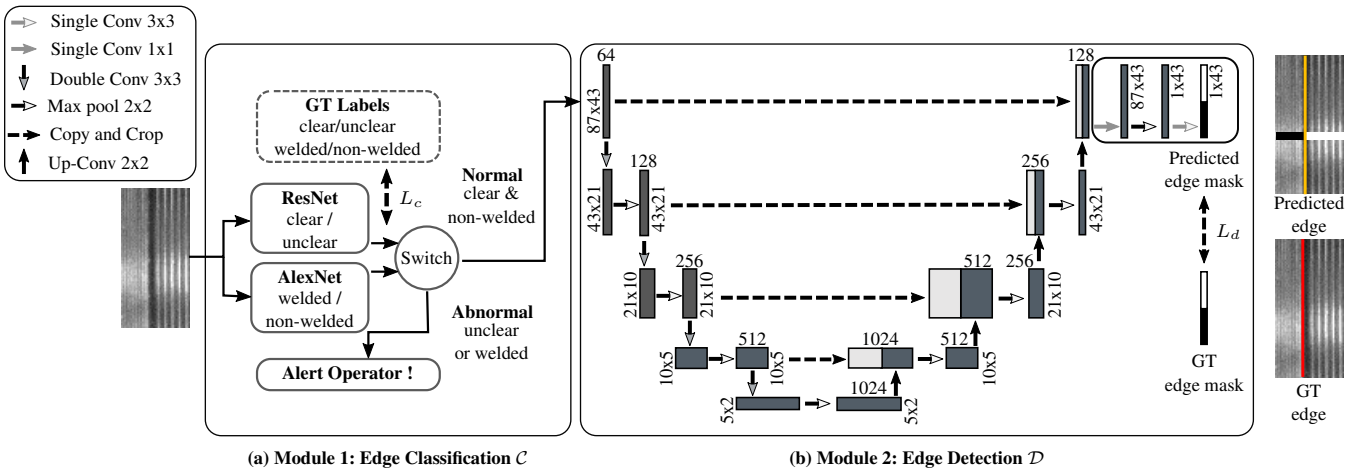

(a) Module 1: Edge Classification $\mathcal{C}$ (b) Module 2: Edge Detection $\mathcal{D}$

Figure 3: (a) Classification module for identification of normal or abnormal edge. If the edge is abnormal, an alert operator informs the worker to stop further processing the input image; otherwise, the second module is given a signal to operate.
(b) Edge detection module, which is a modified U-Net architecture. 3×3 convolution in the second to last layer is replaced with 2×2 max-pooling layer to get 1D output. Input to both modules (a) and (b) is the 87×43 image. The final output of (b) is 1×W, i.e., 1×43, where the boundary between 0s and 1s indicates an edge.

weld seam already exists. A binary cross-entropy loss $L_c(.)$ for N training images is computed as

$$L_c = -\frac{1}{N}\sum_{i=1}^{N} y_i \log(p(y_i)) + (1-y_i)\log(p(1-y_i)). \quad (1)$$

Where y_i is the class label, in our case, either 0 or 1. $p(y_i)$ is the probability of the predicted class.

An alert operator is activated if an edge is unclear or already welded. This marks the image as abnormal and this stops the process and requests human worker intervention. However, if the edge is normal, i.e., both clear and non-welded, processing continues to the next module where a precide edge is detected for welding.

The output of the classification module is given as: $Label_i = \mathcal{C}(I_i)$, where I_i is the i^{th} input image, and $Label_i$ is the normal/abnormal label of corresponding i^{th} image. In experiments section, we explicitly evaluate the effect of employing an edge classification module on the performance of the detection module.

Edge Detection $\mathcal{D}$

The edge detection module is a modified U-Net (Ronneberger, Fischer, and Brox 2015) that takes an input image of size $H \times W$ and outputs a $1 \times W$ binary edge mask. The boundary between 0s and 1s in this mask indicates an edge. First, the 3×3 convolution step in the penultimate layer of the U-Net architecture is replaced with 2×2 max-pooling layer with kernel size 44×1 to get a 1D output. Values in this 1D output vector are then thresholded by 0.5 to obtain an edge mask comprising of 1s and 0s. This modification is highlighted in the top right box of Fig. 3 part (b). This conversion from 2D to 1D simplifies the edge detection task since an edge within our domain is always a line with a vertical gradient. A pixel-wise binary cross-entropy loss $L_d(.)$ is used to train this architecture and is defined as:

$$L_d = -\frac{1}{W}\sum_{i=1}^{W} y_i \log(p(y_i)) + (1-y_i)\log(p(1-y_i)) \quad (2)$$

The loss is calculated for each pixel, i.e., W pixels. The edge detection module $\mathcal{D}$ is only operated on images which pass the classification module $\mathcal{C}$ filter. The output of D is a $Mask_i$ per input image i. This is formalised in equation 3.

$$Mask_i = \begin{cases} \mathcal{D}(I_i), & \text{if } label_i == 1 \\ 0, & \text{otherwise} \end{cases} \quad (3)$$

where I_i is the i^{th} input image, and $label_i$ is the normal/abnormal prediction, $label_i = \mathcal{C}(I_i)$, of the corresponding i^{th} input image.

Experiments and Results

Dataset We present the Laser Seam Detection (LSD) dataset, which consists of 37,952 real-world welding images of size 656×494, see fig. Fig. 4. Out of these, 700 images have weld seams that are visually unclear, and 100 images have seams already welded, as shown in Fig. 4. The already welded seams must be detected and flagged otherwise the worker may incorrectly place them back into the machine. We use the Computer Vision Annotation Tool (CVAT) (Sekachev et al. 2020), an open-source web-based image annotation tool, to manually label the optimum weld seam location. These are verified by professional welding engineers. We use the entire image to label the optimum

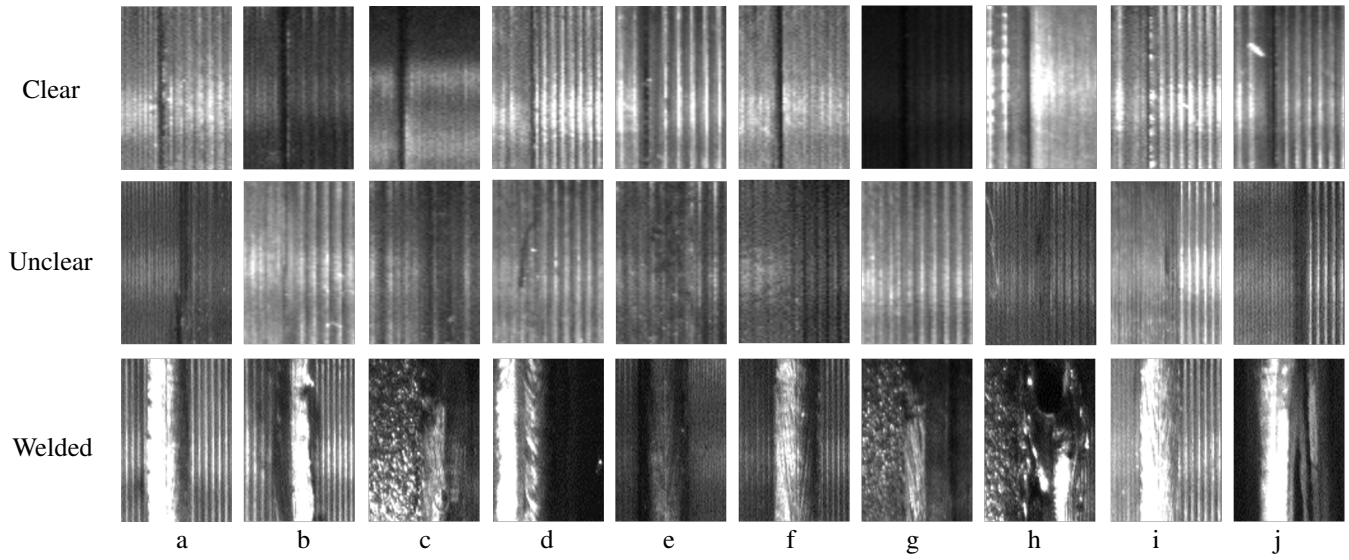

Figure 4: Examples of 'clear', 'unclear', and 'welded' images in the dataset. First row shows normal images with a clear edge, second represents spurious images where an edge is difficult to locate whereas last row has welded images.

weld seam. A complete picture during annotation allows for better visual inspection of the surroundings of the seam area, which helps to discover the optimum seam location within the ROI. The ROI is a fixed central segment of the image with size 87×43. In all our experiments, we only use the cropped ROI of size 87×43 and its corresponding binary edge mask of size 1×43 with 0s before the edge pixel and 1s after for training the network. We label the optimum seam location using a line tool aligned to the y-axis to ensure no diagonal seams are created. We further classify each seam as clear, unclear, welded, or non-welded. All images, along with corresponding labels, will be made publicly available.

Evaluation Metric We report the classification accuracy and confusion matrices for evaluating the classification module $\mathcal{C}$ whereas the edge detection accuracy is reported for the edge detection module $\mathcal{D}$. The edge detection accuracy value is computed given an error threshold of ±1 , ±2 and ±3 pixel left or right deviation from the ground truth seam location. An error of under ±3 pixel satisfies industrial accuracy requirement.

Edge Classification $\mathcal{C}$ Results

We evaluate the classification module using four different popular CNN architectures, namely VGG-16, ResNet-18, LeNet, and AlexNet. A 5-fold cross-validation is performed for each model. Table 1 summarises the results. Two different classification tasks are evaluated; first is the classification of 'clear' vs. 'unclear' image labels and the second is 'welded' vs. 'non-welded images'. The seam is clearly visible to the human eye on all 'clear' images (Fig. 4 first row), whereas it is barely visible on 'unclear' images (Fig. 4 mid row). Moreover, 'clear' images outnumber 'unclear' images. We, therefore, choose equal amounts of 700 of both classes

Model	Clear/ Unclear Accuracy(%)	Welded/ Non-Welded Accuracy(%)
VGG-16	97.1	93.0
ResNet-18	**97.8**	92.0
LeNet	95.4	87.5
AlexNet	96.1	**96.0**

Table 1: Classification Results: The classes are either welded vs. non-welded or clear vs. unclear. We test with several main stream neural networks for this task. Results are average of 5-fold cross-validation. Best results are in bold. The accuracy has been reported in percentage.

to create a balanced dataset. A 90/10 % train/test split is used for training. Table 1 presents a compilation of the achieved results. Note that, ResNet-18 (He et al. 2015) performs best for this task. Under normal circumstances, the image should have an un-welded seam; however, a workpiece with an existing weld seam is occasionally present. We have 100 images with already welded seams. We create an equal dataset of 200 welded and non-welded images followed by a 80/20 % train/test split for training. Despite its simplicity, the best network for this task was surprisingly AlexNet (Krizhevsky, Sutskever, and Hinton 2012), with the highest accuracy as shown in Table. 1.

We also display confusion matrices for both classification tasks in Fig. 5. For this industrial use case, false positives are required to be low since welded or unclear images should not be classified as non-welded or clear, respectively. These misclassifications can result in an incorrect seam being detected and potential damage to the welding machine. Our results clearly show that false positives are avoided to a high

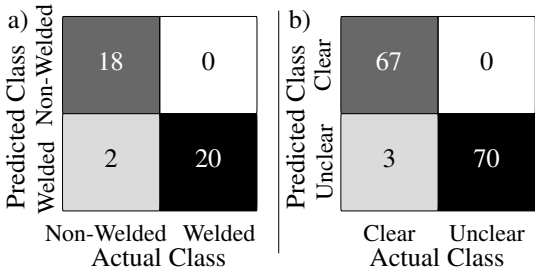

Figure 5: Confusion matrix for (a) welded/non-welded image classification using AlexNet (b) clear/unclear image classification using ResNet-18.

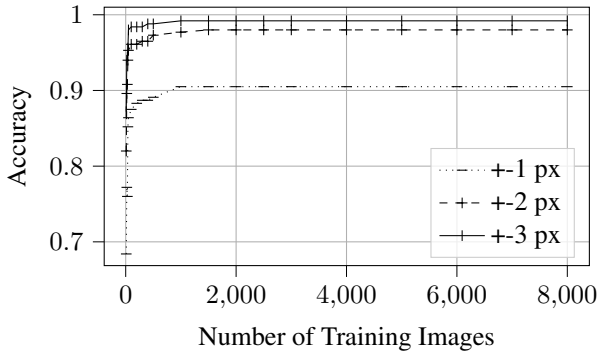

Figure 6: Is more data better? Change in edge detection accuracy with more training images. Clearly, the accuracy on test set saturates after 1500 images.

degree, improving the efficiency of the following edge detection module.

Edge Detection $\mathcal{D}$ Results

We use a shuffled dataset with 'clear' and 'unclear' labeled images to train the edge detection module. Images with already welded edges are not included in training. We isolate 256 randomly selected images for the test set. For the training set, we experiment with increasing number of training images and select an empirically optimum number based on performance increase (see Fig. 6). We train for the same number of training iterations (1286) for each experiment. Fig. 6 confirms that training accuracy of the edge detection module plateaus around 1500 images. Therefore remaining experiments and comparisons are performed with 1500 training images while using the same test set with 256 images.

We compare our modified U-Net architecture with other popular models: VGG (Simonyan and Zisserman 2014), ResNet (He et al. 2015), DenseNet (Huang, Liu, and Weinberger 2016), SegNet (Badrinarayanan, Kendall, and Cipolla 2017), ModSegNet (Ganaye, Sdika, and Benoit-Cattin 2018), DenseASPP (Yang et al. 2018), FastFCN (Wu et al. 2019), OCR (Yuan, Chen, and Wang 2020), and DDRNet (Hong et al. 2021). The training configurations are kept

Model	±1 px Acc	±2 px Acc	±3 px Acc	Inference Time (sec)	Params
VGG	86.7	96.1	**99.2**	0.0052	35.9M
ResNet	84.8	95.3	**99.2**	0.0087	11.3M
DenseNet	84.0	94.9	98.8	0.0326	7.04M
SegNet	88.3	96.5	98.8	0.0074	18.8M
ModSegNet	86.7	94.1	96.9	0.0080	18.9M
DenseASPP	84.0	94.5	98.8	0.0461	10.2M
FastFCN	88.9	97.7	**99.2**	0.0095	26.6M
OCR	83.6	95.7	**99.2**	0.0081	28.6M
DDRNet	82.8	95.3	98.4	0.0052	6.1M
Our modified U-Net	**90.5**	**98.0**	**99.2**	0.0068	17.3M

Table 2: Is U-Net the best architecture for edge detection? Edge detection accuracy in percentage with various deep architectures. Best results are in bold.

System	±1 px Acc	±2 px Acc	±3 px Acc
w/o $\mathcal{C}$	90.5	98.0	99.2
w/ $\mathcal{C}$	**91.7**	**98.8**	**99.4**

Table 3: Effectiveness of edge classification module: Edge detection accuracy in percentage with and without a preclassifier. Best results are in bold.

constant, i.e., 1×W edge mask is set as ground truth, and pixel-wise binary cross-entropy loss is used to train each model. All models are trained for 30 epochs. Visual results of our model are shown in Fig. 7. It can be observed that our method predicts near-perfect edges every time.

Quantitative results, inference time, and model parameters are reported in Table 2. It can be seen that our modified U-Net performs superior compared to all other methods by a large margin. The architectures included have proven to be state of the art on various tasks. However, we notice that modified U-Net is a simple architecture yet performs better.

Effect of Edge Classifier $\mathcal{C}$ on Edge Detector $\mathcal{D}$

For edge detection experiments, we use a test set with 256 images, some of which have unclear or welded images. We report that employing the classification module filters these as abnormal. The remaining test set is then used for edge detection. The results in Table 3 show that adding this filtering improves the edge detection results by about 1.2 % for ± 1 pixel accuracy.

Impact of Preprocessing

We perform additional experiments by applying different image filters to the input image ROI, namely Gaussian filter (GF) and Binary Adaptive Thresholding (ABT) filter. These filters are concatenated as additional input channels for the training of the modified U-Net. We have experimented with four different input configurations. In the first configuration (ROI+GF), four channels are used as input where the ROI image is concatenated with a GF. Another configuration is four-channel (ROI+ABT) input with the ROI image concatenated with the ABT filter. Lastly, a five-channel (ROI+GF+ABT) input configuration is used consisting of the ROI image, GF, and ABT filter. All results are presented

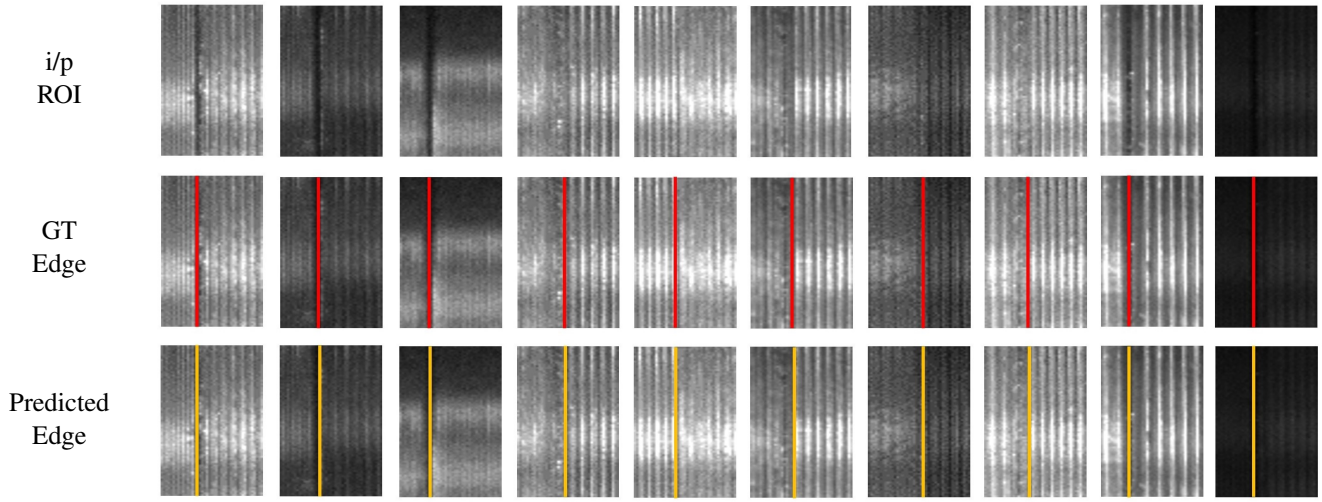

Figure 7: Qualitative Results: Images in the top row represent the input ROI. The second row represents the ROI with the ground truth (GT) edge labeled by CVAT, and the last row shows the edge detected by our modified U-Net architecture. Images have been arranged in increasing order of edge discernment difficulty.

Input	±1 px Acc	±2 px Acc	±3 px Acc
ROI	**90.5**	**98.0**	**99.2**
ROI+GF	87.9	94.0	99.2
ROI+ABT	88.3	96.1	99.2
ROI+GF+ABT	87.2	96.5	98.0

Table 4: Ablations: Edge detection accuracy in percentage with different inputs. Best results are in bold.

in Table 4. We note that adding different image filters does not offer improvement rather degrades it. We assert that this is due to the metallic texture and light glare of the thread surface, which cause visual artifacts resembling vertical lines. These figments confuse the network to detect the true weld seam resulting in inferior performance.

Deployment

Our trained system has been deployed on a Linux-based server that is hosted on-site. Figure 8 shows the details of the entire deployment pipeline. The server runs a Kubernetes cluster which allows for our algorithm to be containerised using docker. The welding machine sends a query image, along with the ROI, to the server using a Rest API call. The docker container receives that image file, processes the image through the U-Net and outputs the optimum edge location. This location is sent back to the machine for welding. Within the server, we also host a monitoring system for a human operator to use in order to track the algorithm's performance. Two main monitoring metrics are employed: data divergence and manual random testing. Data divergence consistently reports the KL-divergence between new data and training data. This is used to detect domain shift. Manual random testing includes a human operator who randomly checks the detected edges for accuracy. These systems ensure a safe and trustworthy deployment.

Application Use and Payoff Our proposed system has been operating in parallel with the worker for over 6 months. The inference time per job is less than 200 ms which matches or surpasses the time taken by a worker. Currently this system has finished 55000 jobs. We also measured the data drift and found that the system does not suffer from data drift due to a controlled environment. Therefore no retraining has been needed so far. Given that such consistent performance maintains for a further 3 months, we expect to transition fully to the automated U-Net system and relieve the worker of this manual task.

Lessons Learned GPU is not needed since we obtain good inference time on CPU alone. Another consideration is that labelling effort should be on a need base only since we manually labelled 8000 images which were clearly not needed as shown in Fig. 6. The use of a Kubernetes cluster model has helped in adopting ML-Ops best practices.

Conclusion

In this paper, we address the task of laser weld seam detection using a customized deep neural network architecture that automatically detects the weld seam between two metals. These metals have been processed by a lathe to a high precision. The system is augmented with a classification module that first classifies input images as normal or abnormal based on the visual clarity of the edge, i.e., whether the weld seam edge in an image is clear and detectable. Our method achieves superior weld seam detection results compared to the standard state-of-the-art deep network architectures. We empirically demonstrate that the proposed method is best suited for this task achieving pixel-level accuracy. We additionally report the amount of labeled data needed to solve similar problems in an industrial setting. We also contribute a unique real-world dataset, complete code, and pretrained models to help further research in this area. Finally,

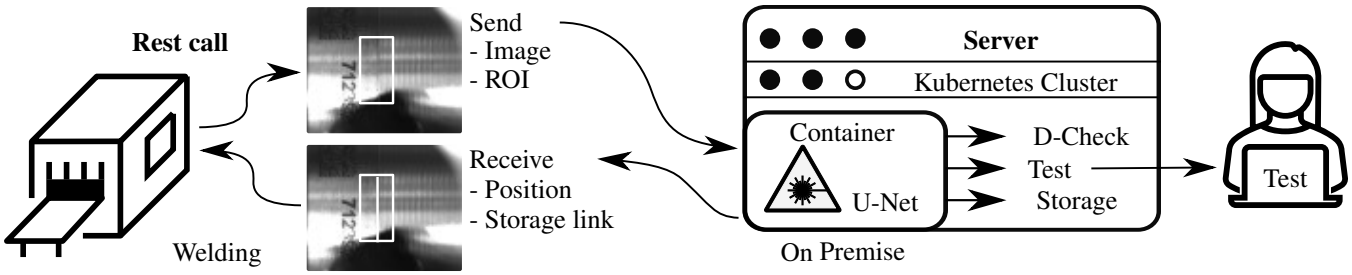

Figure 8: Deployment: Our Server is a linux-based system that runs a Kubernetes cluster with a inference time of 200 ms.

we present a detailed description of our deployment pipeline to bring this system successfully onto the shop floor. Our model's high accuracy allows it to be deployed directly on laser welding machines, saving significant production time and cost.

References

Badrinarayanan, V.; Kendall, A.; and Cipolla, R. 2017. SegNet: A Deep Convolutional Encoder-Decoder Architecture for Image Segmentation. *IEEE Transactions on Pattern Analysis and Machine Intelligence*, 39(12): 2481–2495.

Bastos, T. F.; Martin, J. M.; Calderon, L.; and Ceres, R. 1994. Weld seams detection and recognition for robotic arc-welding through ultrasonic sensors. In *Proceedings of 1994 IEEE International Symposium on Industrial Electronics (ISIE'94)*, 310–315. IEEE.

Dinham, M.; Fang, G.; and Zou, J. J. 2011. Experiments on automatic seam detection for a MIG welding robot. In *International Conference on Artificial Intelligence and Computational Intelligence*, 390–397. Springer.

Ganaye, P.-A.; Sdika, M.; and Benoit-Cattin, H. 2018. Semi-supervised learning for segmentation under semantic constraint. In *International Conference on Medical Image Computing and Computer-Assisted Intervention*, 595–602. Springer.

He, K.; Zhang, X.; Ren, S.; and Sun, J. 2015. Deep Residual Learning for Image Recognition. *CoRR*, abs/1512.03385.

Hong, Y.; Pan, H.; Sun, W.; Jia, Y.; et al. 2021. Deep dual-resolution networks for real-time and accurate semantic segmentation of road scenes. *arXiv preprint arXiv:2101.06085*.

Huang, G.; Liu, Z.; and Weinberger, K. Q. 2016. Densely Connected Convolutional Networks. *CoRR*, abs/1608.06993.

Krizhevsky, A.; Sutskever, I.; and Hinton, G. E. 2012. ImageNet Classification with Deep Convolutional Neural Networks. In *Proceedings of the 25th International Conference on Neural Information Processing Systems - Volume 1*, NIPS'12, 1097–1105. Red Hook, NY, USA: Curran Associates Inc.

Li, X.; Li, X.; Ge, S. S.; Khyam, M. O.; and Luo, C. 2017. Automatic Welding Seam Tracking and Identification. *IEEE Transactions on Industrial Electronics*, 64(9): 7261–7271.

Lu, J.-Y.; Pan, H.-P.; and Xia, Y.-M. 2013. The weld image edge-detection algorithm combined with Canny operator and mathematical morphology. In *Proceedings of the 32nd Chinese Control Conference*, 4467–4470.

Micallef, K.; Fang, G.; and Dinham, M. 2011. Automatic seam detection and path planning in robotic welding. In *Robotic welding, intelligence and automation*, 23–32. Springer.

Pachidis, T. P.; and Lygouras, J. N. 2007. Vision-based path generation method for a robot-based arc welding system. *Journal of Intelligent and Robotic Systems*, 48(3): 307–331.

Pan, J. 2001. Arc sensing system for automatic weld seam tracking (II). *Science in China Series E: Technological Sciences*, 44(4): 389–397.

Ronneberger, O.; Fischer, P.; and Brox, T. 2015. U-Net: Convolutional Networks for Biomedical Image Segmentation. *CoRR*, abs/1505.04597.

Rout, A.; Deepak, B.; and Biswal, B. 2019. Advances in weld seam tracking techniques for robotic welding: A review. *robotics and computer-integrated manufacturing*, 56: 12–37.

Ryberg, A.; Ericsson, M.; Christiansson, A.-K.; Eriksson, K.; Nilsson, J.; and Larsson, M. 2010. Stereo vision for path correction in off-line programmed robot welding. In *2010 IEEE International Conference on Industrial Technology*, 1700–1705. IEEE.

Sekachev, B.; Manovich, N.; Zhiltsov, M.; Zhavoronkov, A.; Kalinin, D.; Hoff, B.; TOsmanov; Kruchinin, D.; Zankevich, A.; DmitriySidnev; Markelov, M.; Johannes222; Chenuet, M.; a andre; telenachos; Melnikov, A.; Kim, J.; Ilouz, L.; Glazov, N.; Priya4607; Tehrani, R.; Jeong, S.; Skubriev, V.; Yonekura, S.; vugia truong; zliang7; lizhming; and Truong, T. 2020. opencv/cvat: v1.1.0. *Zenodo*.

Simonyan, K.; and Zisserman, A. 2014. Very deep convolutional networks for large-scale image recognition. *arXiv preprint arXiv:1409.1556*.

Wu, H.; Zhang, J.; Huang, K.; Liang, K.; and Yu, Y. 2019. Fastfcn: Rethinking dilated convolution in the backbone for semantic segmentation. *arXiv preprint arXiv:1903.11816*.

Wu, Q.-Q.; Lee, J.-P.; Park, M.-H.; Jin, B.-J.; Kim, D.-H.; Park, C.-K.; and Kim, I.-S. 2015. A study on the modified Hough algorithm for image processing in weld seam tracking. *Journal of Mechanical Science and Technology*, 29(11): 4859–4865.

Xiong, Y.; Shi, F.; Lin, T.; and Chen, S. 2009. Efficient weld seam detection for robotic welding based on local image processing. *Industrial Robot: An International Journal*.

Yang, M.; Yu, K.; Zhang, C.; Li, Z.; and Yang, K. 2018. Denseaspp for semantic segmentation in street scenes. In *Proceedings of the IEEE conference on computer vision and pattern recognition*, 3684–3692.

Yuan, Y.; Chen, X.; and Wang, J. 2020. Object-contextual representations for semantic segmentation. In *Computer Vision–ECCV 2020: 16th European Conference, Glasgow, UK, August 23–28, 2020, Proceedings, Part VI 16*, 173–190. Springer.

Zeng, J.; Chang, B.; Du, D.; Hong, Y.; Chang, S.; and Zou, Y. 2016. A precise visual method for narrow butt detection in specular reflection workpiece welding. *Sensors*, 16(9): 1480.

Zou, Y.; and Chen, T. 2018. Laser vision seam tracking system based on image processing and continuous convolution operator tracker. *Optics and Lasers in Engineering*, 105: 141–149.

Zou, Y.; and Zhou, W. 2019. Automatic seam detection and tracking system for robots based on laser vision. *Mechatronics*, 63: 102261.